# Chaotic patterns in a Josephson junction model

O. H. Olsen

*Biostructure Department, Novo-Nordisk Research Institute, DK-2880 Bagsværd, Denmark*
(Received 1 February 1994)

The effect of an applied rf signal on the dynamics of a large area Josephson junction is examined by means of a model based on the sine-Gordon equation. In particular the problem of characterizing spatiotemporal chaotic patterns induced by the external harmonic varying magnetic field is addressed. In general it is found that instantaneous spatiotemporal patterns, i.e., patterns confined to one period of oscillation of the external field correlates poorly. Also the correlation between instantaneous patterns and average patterns is poor. However, the correlation between patterns obtained as averages over, e.g., ten or more consecutive instantaneous spatiotemporal patterns is high. Furthermore, averaged spatiotemporal patterns obtained for different values of the magnetic field amplitude correlate well. The average potential and kinetic energies of spatiotemporal patterns are calculated. In general the energies in the chaotic regions are lower than in regions with periodic response.

PACS number(s): 05.45.+b, 74.40.+k, 52.35.Mw, 03.40.Kf

## I. INTRODUCTION

There has been an increasing interest in properties of systems that show spatiotemporal chaos, with large fluctuations in space and time. Recently investigations dealing with the analysis of spatiotemporal chaotic systems [1,2] have shown that such patterns can have highly ordered time averages. Experiments such as a rotating Rayleigh-Benard system [1] and a Faraday instability in large fluid layers [2] were considered. In [1], ordered time-averaged patterns in the presence of large fluctuations were determined quantitatively. The effects persisted far into the chaotic regime. Similar results were found in [2]. It is intriguing that the application of a simple statistical measure, i.e., time averaging of fluctuating patterns, shows highly ordered average patterns.

Previously [3–5], the influence of an applied rf signal on the radiation emitted from a long Josephson junction was examined theoretically. The study of the dynamical behavior of long Josephson junctions is of fundamental as well as practical interest. From a theoretical point of view the system shows a rich variation of nonlinear properties which are suitable for detailed investigations of, e.g., nonlinear wave dynamics and chaotic states [6–10]. From an applications point of view there have been suggestions for the use of Josephson junctions in such diverse fields as microwave-oscillator amplifiers and data-processing systems. The Josephson junction model was based on the sine-Gordon equation. The microwave pump signal was applied to one end of the junction. Thus the system was modeled by a perturbed one-dimensional sine-Gordon equation with appropriate boundary conditions describing the influence of the rf signal. The rms value of the voltage of the emitted signal was calculated and used to evaluate the response of the junction. Various interesting phenomena were found depending on the amplitude of the rf signal: period doubling sequences or bifurcation trees (devils staircase), chaos, quasiperiodicity, and hysteresis. Further, for particular values of the

applied frequency the following scenario was observed [5]: for small and large values of the applied amplitude the system response was periodic. The periodic patterns observed in the two regions were different—the dynamics in the transition region from one pattern to the other were characterized as chaotic. Seen in the light of the recent investigations [1,2] of spatiotemporal chaotic systems, the described scenario observed in the Josephson junctions model is a case where chaotic patterns can be compared to periodic patterns. Further, energies can be calculated based on the Hamiltonian defining the system.

The aim of the present work is to study the spatiotemporal patterns generated in the Josephson junction system described above. The dynamics of the system at one frequency $\omega_0 = 0.7$ is considered when the amplitude $a$ is varied. For values of $a \leq 1.46$ and $a \geq 1.92$ the response is periodic, frequency locked to the driver signal. The mode sustaining the periodic response for $a \leq 1.46$ was identified as a breatherlike mode [4]. Between these two values the response is chaotic supposedly due to a competition between different patterns [3]. Inspired by the results in [1,2] we analyze the patterns in the chaotic as well as in the region with periodic time response. We find that instantaneous spatiotemporal patterns (i.e., patterns confined to one period of oscillation of the external magnetic field) in the chaotic region correlate poorly. The correlation between instantaneous patterns and average patterns is also rather poor. A much better correlation is found between average patterns (obtained from, e.g., $j$ consecutive patterns, $j$ being in the range 2–100). Further, the correlation between average patterns obtained for different values of the amplitude is high. In the chaotic region the potential as well as the kinetic energies drop compared to the energies of the periodic patterns.

The paper is outlined as follows: Section II contains a description of the model, the numerical procedure, and some examples of spatiotemporal patterns. In Sec. III the results are presented. Finally, Sec. IV contains a discussion.

## II. MODEL AND NUMERICAL METHOD

In the present section the model used to describe the dynamical behavior of long Josephson junctions is outlined, and examples of spatiotemporal patterns are presented.

### A. Model

The mathematical model used to describe the dynamics of a long Josephson junction is a perturbed sine-Gordon equation. The perturbation includes a dissipation term. In normalized form the equation is

$$\varphi_{xx} - \varphi_{tt} = \sin\varphi + \alpha\varphi_t \, , \tag{1}$$

where $\varphi(x,t)$ is the superconducting phase difference between the electrodes of the junction, the spatial coordinate $x$ is normalized to the Josephson penetration depth $\lambda_J$, the time $t$ is normalized to the inverse plasma frequency $\Omega_0^{-1}$, and $\alpha$ is the dissipation coefficient. The loss parameter models dissipative currents (quasiparticle currents).

If an oscillating magnetic field $H_e\sin\omega_0 t$ is applied to one end (in this case the right end) of the junction, perpendicular to the length of the junction and parallel to the plane of the barrier, the boundary conditions for the phase difference $\varphi$ at the ends are

$$\varphi_x(0,t) = 0, \quad \varphi_x(l,t) = a \sin\omega_0 t \, , \tag{2}$$

where $a = H_e/J\lambda_J$ and $l = L/\lambda_J$ are the normalized magnetic-field strength and junction length, respectively. The external magnetic field is assumed to influence only the boundary condition and not Eq. (1), which describes the dynamics of the interior of the junction.

### B. Numerical methods

The numerical procedure applied to solve the system described by Eq. (1) with the boundary conditions given by Eqs. (2) is based on a "leap-frog" scheme [11]. The spatial discretization step was $dx = 0.05$ (the corresponding time step was $dx/2$). In Fig. 1 we show the results of such a solution in terms of the rms value $\langle\varphi_t^2\rangle^{1/2}$ (at $x = l$) as a function of the applied amplitude $a$. The specific parameter values in Fig. 1 are frequency $\omega_0 = 0.7$ and length $l = 5$. The loss parameter ($\alpha = 0.2$) is held fixed. In order to stimulate an experimental situation we follow the procedure from [5]. Thus for $a = 0$ we use flat initial conditions [$\varphi(x,0) = 0$ and $\varphi_x(x,0) = 0$], and $a$ is then increased gradually by an amount $\Delta a$ [using a ramp function $a_{\text{new}} = a_{\text{old}} + (\Delta a/50)t$ for $t < 50$]. The steady state is typically obtained after $t = 100$, and each run is continued to $t = 15\,000$. After calculation of the last eight rms values, $\langle\varphi_t^2\rangle^{1/2}$, the computations are stopped and restarted, (the initial conditions now being the previous solution), and $a$ is gradually increased. This procedure is continued for $a < 2.0$ with $\Delta a = 0.005$. Note that the rms value $\langle\varphi_t^2\rangle^{1/2}$ is defined as the square root of the following quantity:

$$\langle\varphi_t^2\rangle = \frac{\omega_0}{2\pi} \int_{t_0}^{t_0 + (2\pi/\omega_0)} \varphi_t^2 dt \, , \tag{3}$$
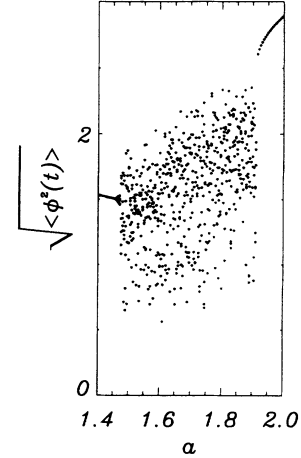


FIG. 1. The rms value $\langle\varphi_t^2\rangle^{1/2}$ vs the applied amplitude $a$. Parameter values are $l = 5$, $\alpha = 0.2$, and $\omega = 0.7$. The amplitude has been increased from 1.4 to 2.0 in steps of $\Delta a = 0.005$. For values of $a \leq 1.46$ and $a \geq 1.92$, the response is periodic. The set of scattered points indicates chaotic time response. The units of the various parameters and variables are defined in the text.

where $t_0$ is the time for a positive zero crossing of $\varphi_x(l,t)$ [i.e., $\varphi_x(l,t)$ changes from a negative value to a positive]. In Fig. 1 the resulting curve is shown for $1.4 \leq a \leq 2.0$. In this region no hysteresis is observed in contrast to what is found for $0.75 \leq a \leq 1.16$ [5]. For each value of $a$, eight consecutive values of the rms value of $\varphi_t$ have been plotted. This allows the identification of regions with periodic dynamics as well as regions with chaotic dynamics. In Fig. 1 it can be seen that the rms value changes rapidly for $a = 1.46$, which corresponds to a change in the wave dynamics. For $1.46 < a < 1.92$ the resulting dynamics give a scattered set of dots corresponding to a chaotic time response. The response is again periodic for $a > 1.92$. In the regions where the response is periodic, the phase $\varphi$ oscillates around a fixpoint $2\pi n$. However, in the chaotic region the phase jumps between fixpoints.

In Figs. 2–4 examples of spatiotemporal patterns for $a = 1.4$, 1.7, and 2.0 are shown in terms of the spatial derivative $\varphi_x(x,t)$. Thus examples of patterns from the periodic regions as well as from the chaotic region are shown. Dotted and full lines correspond to positive and negative values of $\varphi_x(x,t)$. Furthermore, the dot-dashed lines correspond to $\varphi_x(x,t) = 0$. The external magnetic field has been shown to the right of the patterns. Power spectra are also shown. The power spectra are calculated from the last 10 000 time units of $\varphi_t(l,t)$. In Fig. 2 the response is clearly periodic, which is also supported by the power spectrum. Figure 3 shows an example of chaotic response, again supported by the power spectrum. Finally, in Fig. 4 an example of the spatiotemporal pattern in the region $a > 1.92$ is shown.

In order to analyze the spatiotemporal patterns, average patterns are calculated. Because the phase $\varphi$ jumps in the chaotic region, the patterns are analyzed in terms of $\varphi_x(x,t)$ ($\cos\varphi$ might also have been used). One spatiotemporal pattern is confined to one period of oscilla-
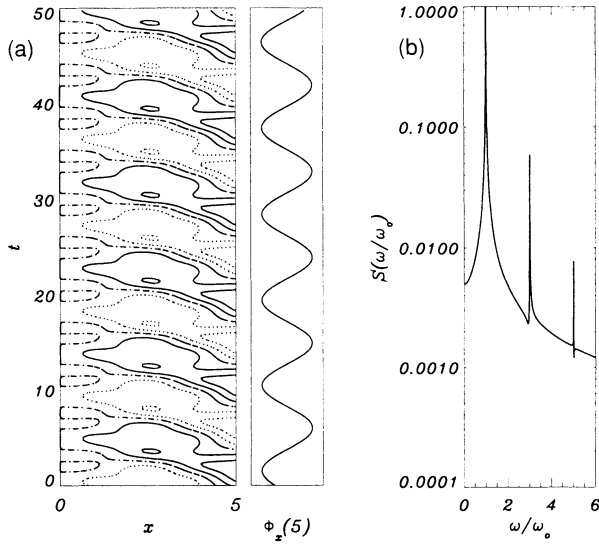
FIG. 2. Periodic time response. Parameter values as in Fig. 1, $a = 1.4$. In (a) the periodic spatial-temporal pattern is shown in terms of the spatial derivative $\varphi_x(x,t)$. The external force is shown to the right for reference. In (b) the corresponding power spectrum is shown. The units of the various parameters and variables are defined in the text.

FIG. 4. Periodic time response. Parameter values as in Fig. 1, $a = 2.0$. In (a) the periodic spatial-temporal pattern is shown in terms of the spatial derivative $\varphi_x(x,t)$. The external force is shown to the right for reference. In (b) the corresponding power spectrum is shown. The units of the various parameters and variables are defined in the text.

tion of the external magnetic field. Thus a pattern consists of $N = (l/dx) + 1$ times $M = (2\pi/\omega_0 dx) + 1$ points, $N$ and $M$ being the number of spatial and temporal grid points, respectively. These points are transformed (by interpolation) to the same grid points within one period of oscillation [i.e., $t_{\text{grid},m} = t_0 + (m-1)dx, m = 1, M$]. Dur-
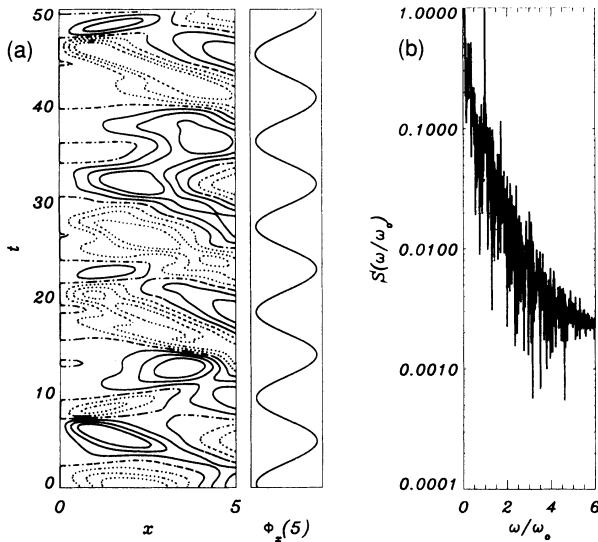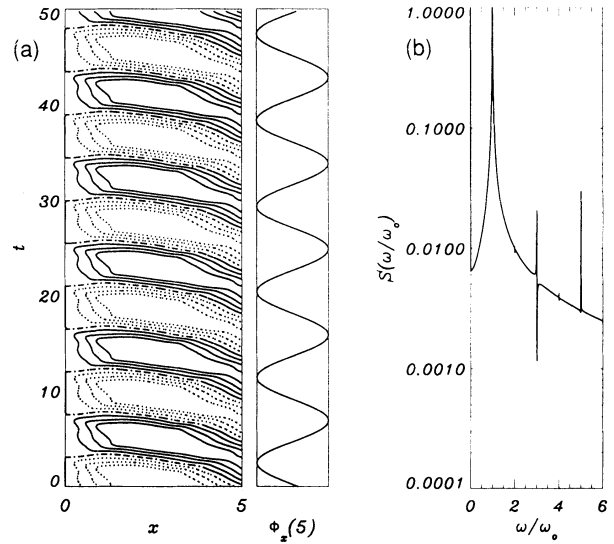
FIG. 3. Chaotic time response. Parameter values as in Fig. 1, $a = 1.7$. In (a) the chaotic spatial-temporal pattern is shown in terms of the spatial derivative $\varphi_x(x,t)$. The external force is shown to the right for reference. In (b) the corresponding power spectrum is shown. The units of the various parameters and variables are defined in the text.

ing the simulations described above, patterns are saved. The first 50 periods are discarded. Then two procedures are followed. In the *first* procedure $k$ average patterns $A_{k,j}(n,m)$, produced from $j$ consecutive instantaneous patterns, are generated. These patterns are then cross correlated. In the *second* procedure an average pattern $A(n,m)$ is generated from the first 200 periods of oscillation. After these 200 periods the correlation between an instantaneous pattern $I(n,m)$ and the previously generated average pattern is calculated. Further, after calculation of the correlation coefficient the instantaneous pattern is accumulated in the average pattern. For each instantaneous pattern the correlation coefficient is calculated. Finally, for each value of $a$ the average value of the correlation coefficient and standard deviation is then calculated. The formula used to calculate the correlations in the *second* procedure is

$$c = \frac{\sum\limits_{n=1}^{n} \sum\limits_{m=1}^{M} I(n,m) A(n,m)}{\left[ \sum\limits_{n=1}^{N} \sum\limits_{m=1}^{M} I^2(n,m) \right]^{1/2} \left[ \sum\limits_{n=1}^{N} \sum\limits_{m=1}^{M} A^2(n,m) \right]^{1/2}} . \tag{4}$$

Using this formula the correlation coefficient between the patterns shown in Figs. 2 and 4 is 0.873. A similar formula is used to calculate the cross correlations from average patterns obtained in the *first* procedure.

For each instantaneous pattern the kinetic and potential energies are calculated. The kinetic energy is given by

$$E_{\text{kin}} = \frac{1}{2} \int_{t_0}^{t_0 + (2\pi/\omega_0)} \int_0^l \varphi_t^2 dx \, dt , \tag{5}$$

and the potential energy by

$$E_{\text{pot}} = \int_{t_0}^{t_0 + (2\pi/\omega_0)} \int_0^l [\tfrac{1}{2}\varphi_x^2 + (1 - \cos\varphi)]\,dx\,dt \ . \tag{6}$$

Furthermore, the energy dissipation

$$E_{\text{loss}} = -\alpha \int_{t_0}^{t_0 + (2\pi/\omega_0)} \int_0^l \varphi_t^2\,dx\,dt \tag{7}$$

and energy input

$$E_{\text{in}} = \int_{t_0}^{t_0 + (2\pi/\omega_0)} \varphi_x(l,t)\varphi_t(l,t)\,dt \tag{8}$$

in one period of oscillation are calculated. In Sec. III results from the analysis described above are presented.

## III. ANALYSIS OF SPATIOTEMPORAL PATTERNS

First, in this section, patterns generated at a specific value of the amplitude of the applied external field $a = 1.7$ are investigated. This value corresponds to a point placed in the middle of the chaotic region (see Fig. 1). Second, the patterns generated for $1.4 \le a \le 2.0$ are analyzed. Finally, the energies of the chaotic and the periodic patterns are compared.

### A. Amplitude $a = 1.7$

To better understand the averaged patterns the following question is posed: How well do average patterns obtained for the same values of frequency and amplitude of the applied signal correlate? A number of $k = 25$ average patterns consisting of a varying number of consecutive instantaneous patterns are generated. The number of instantaneous patterns $j$ used to generate the average patterns varies from 2 to 100. The average patterns obtained for each number are then cross correlated. In Fig. 5 the results are shown in terms of probability densities of the correlation coefficients $c$. The density labeled I corresponds to the correlation of patterns averaged over two
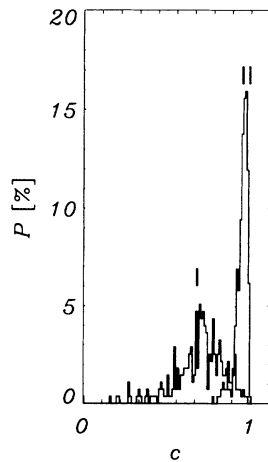


FIG. 5. Probability densities of cross correlation coefficients $c$. The density labeled I corresponds to the correlation between patterns averaged over two consecutive instantaneous patterns, while the density labeled II corresponds to correlations between patterns averaged over ten consecutive patterns.

instantaneous patterns, while the density labeled II corresponds to correlations between patterns averaged over ten consecutive patterns. The density labeled I has a shape not far from Gaussian and an average value $\langle c \rangle = 0.69$; the standard deviation is $\sigma(c) = 0.15$. The correlation between averaged patterns increases drastically with the number of consecutive patterns. For $j = 10$ the average correlation coefficient is 0.93. Now in Fig. 6 the average values $\langle c \rangle$ and standard deviations $\sigma(c)$ for the cross-correlated average patterns are shown as a function of the number of instantaneous patterns $j$ used to generate the averages. If $j$ is increased to 100, the correlation coefficient increases to 0.99, i.e., the average patterns are virtually identical. From the observed densities of correlation coefficients no evidence is found that states very close to the average pattern occur.

### B. Amplitude $1.4 \le a \le 2.0$

Now the correlation between instantaneous patterns and averaged patterns obtained in the *second* procedure are analyzed for $a$ in the interval from 1.4 to 2.0. In Fig. 7 the average correlation coefficients $\langle C \rangle$ (diamonds) and the standard deviations (dots) are shown vs the amplitude of the applied field $a$. Further, the cross correlations between patterns averaged over 100 consecutive instantaneous patterns are shown as the dashed line ($\langle c \rangle = 0.99$). When $a = 1.455$ the response changes from regular to chaotic dynamics, resulting in a decrease in the average correlation $\langle C \rangle$ from 1 to 0.78. A similar behavior is observed for $a = 1.93$ when the upper region for periodic response is entered. The standard deviation in the chaotic region is close to 0.1, indicating a probability distribution corresponding to I in Fig. 5. Note that the correlation increases when the onset for periodic response is approached.

For each value of $a$ an average pattern has been stored (averaged over all patterns except the first 50 patterns). In Fig. 8 correlation coefficients $C_{\text{av}}$ between average patterns are shown vs $a$. The diamonds correspond to the correlation between the average pattern obtained for $a = 1.4$ and patterns obtained for $a \ge 1.4$ while the dots correspond to the correlation between the average pattern obtained for $a = 2.0$ and patterns obtained for
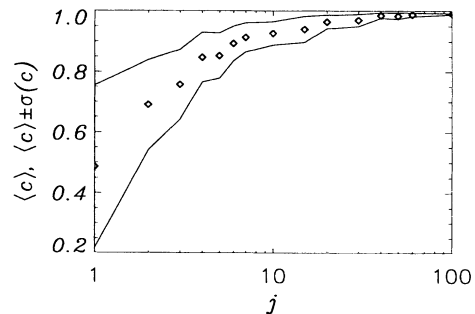


FIG. 6. Average values $\langle c \rangle$ (diamonds) and standard deviations $\sigma(c)$ (dots) for the cross-correlated average patterns are shown as a function of the number of patterns $j$. The amplitude $a = 1.7$.
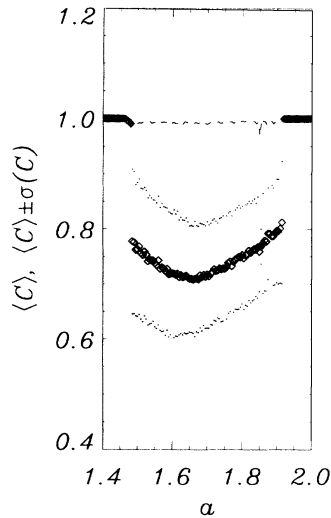
FIG. 7. Correlation coefficients vs $a$. The diamonds correspond to the average correlation coefficients between instantaneous patterns and average patterns, while the dashed curve corresponds to correlations between average patterns (from 100 consecutive patterns). The dots indicate the standard deviation for correlation coefficients between instantaneous patterns and average patterns. The units of the various parameters and variables are defined in the text.

$a \leq 2.0$. This figure indicates that the average patterns obtained in the chaotic region are more similar to the patterns observed in the periodic region for smaller values of $a$ than the patterns observed in the periodic region for larger values of $a$.
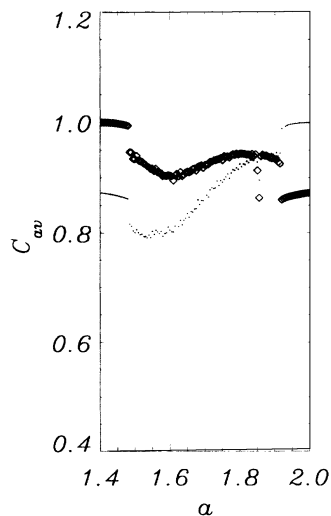
FIG. 8. Correlation coefficients between average patterns vs $a$. The diamonds correspond to the correlation between the average pattern obtained for $a = 1.4$ and patterns obtained for $a \geq 1.4$, while the dots correspond to the correlation between the average pattern obtained for $a = 2.0$ and patterns obtained for $a \leq 2.0$. The units of the various parameters and variables are defined in the text.
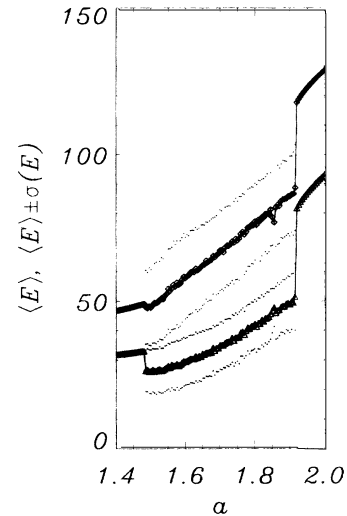
FIG. 9. Average potential and kinetic energies vs $a$. The diamonds and triangles correspond to average potential (upper curve) and kinetic (lower curve) energies, respectively. A line through the average points have been drawn to guide the eyes. The dots indicate the standard deviation. The units of the various parameters and variables are defined in the text.

## C. Energy variation

As mentioned above, various energy terms have been calculated for the instantaneous patterns [Eqs. (5)–(8)]. In Fig. 9 average potential and kinetic energies vs $a$ are shown. Diamonds and triangles correspond to average potential (upper curve) and average kinetic (lower curve) energies, respectively. The dots indicate the standard deviation. Again drops are observed when the chaotic region is entered. The average potential and kinetic energies decrease in the chaotic region compared to regions with periodic response. However, the energy difference between periodic and chaotic patterns is largest for large values of $a$, in accordance with observations in Fig. 8. Thus the modes sustaining the regular response have a higher energy than the chaotic modes in the present system. From that it also follows that the energy input and energy loss is reduced in the chaotic region compared to the ordered region. On average, the energy input and energy dissipation will of course balance.

## IV. DISCUSSION

In this paper some simple statistical properties of spatiotemporal chaotic patterns have been investigated. Time averaged patterns (averaged over, e.g., 10–100 consecutive instantaneous patterns) are ordered in the sense that they are highly correlated. Thus averaged patterns are virtually identical. In the present example periodic patterns observed for small values of $a$ are more correlated to the average patterns obtained in the chaotic region than the periodic pattern found for large values of $a$.

The average potential and kinetic energies are lower in the chaotic region compared to the periodic regions. Thus the modes sustaining the periodic response are

more energy rich than the chaotic modes.

One reason for the relatively high correlation coefficients (virtually no negative coefficients are observed) is the presence of the harmonic external field. The reason for the high correlation between average patterns might be a slow (and almost periodic) variation in the chaotic regime. Such a slow mode has not been identified.

The reasons for observations of highly ordered average patterns remain an open question.

[1] B. J. Gluckman, P. Marcq, J. Bridger, and J. P. Gollup, Phys. Rev. Lett. **71**, 2034 (1993).

[2] L. Ning, Y. Hu, R. E. Ecke, and G. Ahlers, Phys. Rev. Lett. **71**, 2216 (1993).

[3] O. H. Olsen and M. R. Samuelsen, Phys. Lett. **119**, 391 (1987).

[4] O. H. Olsen and M. R. Samuelsen, Phys. Rev. B **34**, 3510 (1986).

[5] O. H. Olsen and M. R. Samuelsen, Phys. Rev. B **43**, 10273 (1991).

[6] P. S. Lomdahl, O. H. Sorensen, and P. L. Christiansen, Phys. Rev. B **25**, 5737 (1982).

[7] A. R. Bishop, K. Fesser, P. S. Lomdahl, and S. E. Trullinger, Physica **7D**, 259 (1983).

[8] D. W. McLaughlin and A. C. Scott, Phys. Rev. A **18**, 1652 (1978).

[9] M. Octavio and L. E. Guerrero, Phys. Rev. A **42**, 4630 (1990).

[10] Y. S. Kivshar and B. A. Malomed, Rev. Mod. Phys. **61**, 762 (1989).

[11] R. K. Dodd, J. C. Eilbeck, J. D. Gibbon, and H. C. Morris, *Solitons and Nonlinear Wave Equations* (Academic, London, 1982), p. 581.